Online Supplemental Material

Fig. S1. **Sites of mutation in the PDZ binding pockets of NHERF1 cDNAs.**
To gain insight into the mechanisms involved in NHERF1-induced metastatic cellular phenotype, we stably transfected the human breast metastatic cell line, MDA-MB-231, with either wild-type (WT) NHERF1 or with NHERF1 in which the binding groove consensus sequence has been mutated from GYGF to GAGA of either the PDZ1 (PDZ1mut) or PDZ2 (PDZ2mut) domains. As a control, the parental MDA-MB-231 cells were transfected with the empty vector (pcDNA).

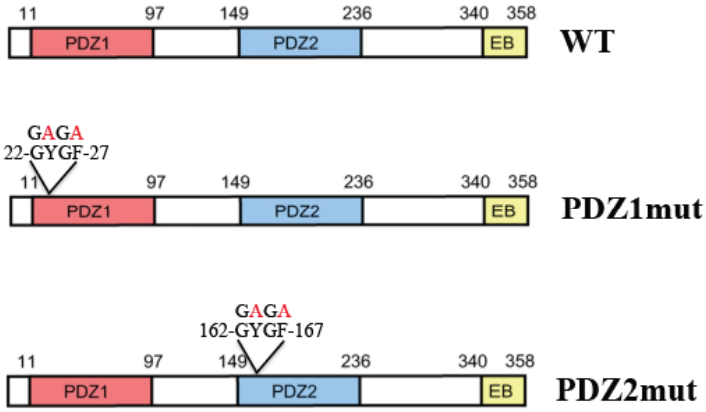

The structure (Karthikeyan et al., 2001) and explanation of the 3D dynamics of the binding of a protein partner to PDZ1 was presented for ß2-Adrenergic and PDGF Receptors (Karthikeyan et al., 2002) but the concept is identical for all binding partners and for the PDZ2 domain. The side chains and carboxylate group of a binding protein (eg. the C-terminal NDSLL of ßAR and EDSFL of PDGFR) enter into a deep cavity formed, in PDZ1, by Gly23, Tyr24, Gly25, Phe26, Leu28 and on the other side of the loop Val76 and Ile79 residues. An indication of the importance of these residues is indicated in the conserved mirroring of these residues and structure in the PDZ2 domain. These residues were then used to block pocket binding (Khundmiri et al., 2005, 2008) and the authors found that the mutation of GYGF to GAGA was the most efficient set of mutations to no longer permit binding of other proteins while having very little or no effect on other characteristics of the expressed protein.

Fig. S2. Production of stable clones and NHERF1 intracellular distribution. Twenty five clones were isolated for each cDNA and tested in **(A)** Immunofluorescence with anti-6his labeling, Bar, 20μm and with **(B)** Western Blotting with anti-NHERF1 antibody. From these preliminary experiments, 3 clones were selected based on levels of transfected ectopic NHERF1 expression similar to those previously observed (Cardone et al., 2007) in which NHERF1 endogenous expression was increased approximately three-fold by transient transfection.
These semi-final three clones of each cDNA were further screened on the basis of: (**C**) their anchorage-independent growth on soft agar; **(D)** their invasive capacity in Boyden Chambers; **(E)** their NHE1 activity by spectrofluorimetric measurements and **(F)** the expression of phospho-RhoA and phospho-p38. Those clones, whose NHE1 activity, invasion, and invasive signal transduction pattern were identical to the transiently transfected cells (Cardone et al., 2007) indicating that no erratic epigenetic alterations in behavior, physiology and biochemistry had occurred with stable transfection, were afterwards analyzed for **(G)** NHERF1 intracellular localization by confocal IF analysis. NHERF1 fluorescence is shown in red, while the actin cytoskeleton was marked with FITC-phalloidin (green). Bar, 10μm.

On the basis of all these measurements single clones for each WT-NHERF1 and PDZ1 or PDZ2 mutated NHERF1 constructs were selected in order to conduct all the subsequent experiments. Data are presented as mean ± s.e.m.; ANOVA vs pcDNA.

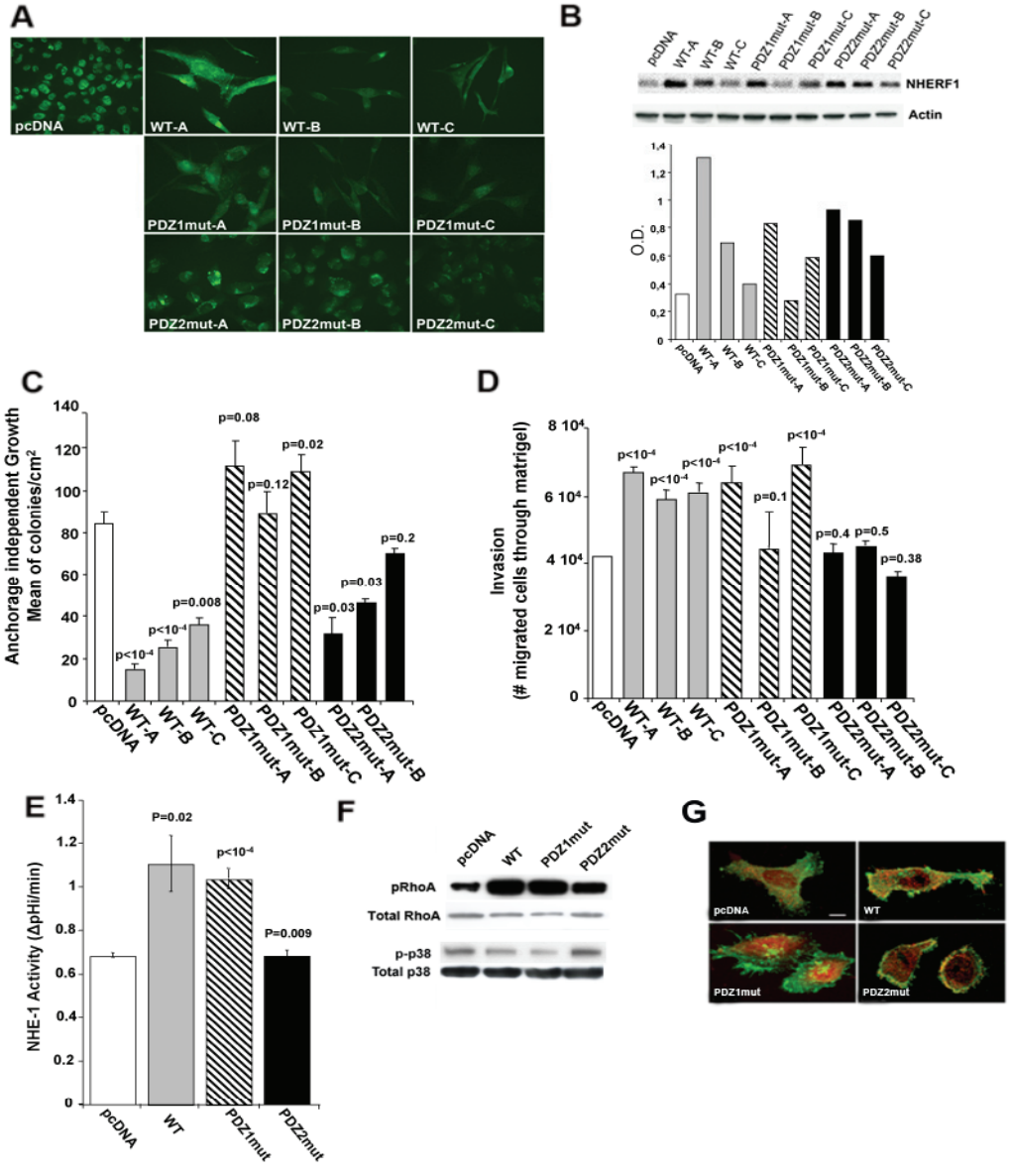

Fig. S3. NHERF1 mutant expression alters tumor motility. Wound healing assay was used to study the effect of NHERF1 expression levels and mutation on cell migration. The recolonization of wounded areas was studied using an inverted phase-contrast microscope from t0 (top) to 24 hrs (bottom). Images shown are representative of three independent experiments. Monolayers from pcDNA and PDZ2mut overexpressing cells showed fast wound healing within 24 hr but those WT and PDZ1mut overexpressing cells showed clear wound width at 24 hr.

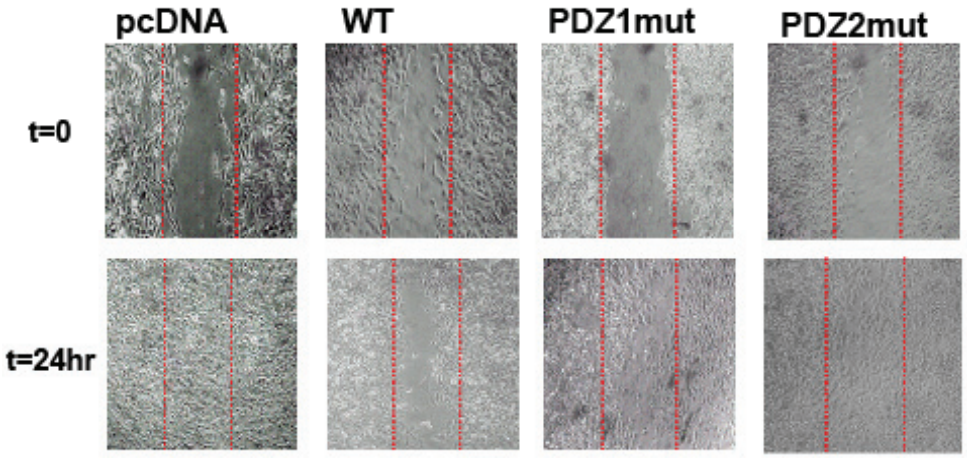

Fig. S4. Measurements of epithelial vs mesenchymal 'markers' in pcDNA, WT, HRF1 and HRF2 cells. As epithelial and mesenchymal cells differ in their cytosketelal architecture as well as in the expression of various epithelial and mesenchymal markers (Hugo et al., 2007; Chao et al., 2010), cells from the four cell variants were seeded on Matrigel^{TM} for 24 hrs and tested for (**A)** cell morphology and stress fiber formation by using phalloidin to visualize the stress fibers organization (left panel, Bar, 10μm) and calculating the Percentage of F-actin stress fibers positivity for each cell line as the number of F-actin stress fibers positive cells over the total number of cells in each field (right panel). PDZ2mut cells showed a reversion of the WT and PDZ1mut fibroblast-like phenotype in a cuboidal-like phenotype with a drastic disarray of the F-actin stress fibers; and **(B)** expression in Western Blot for protein markers of epithelial and mesenchymal phenotypes with the following antibodies: monoclonal antibody anti-smooth muscle actin (Sigma), monoclonal anti-vimentin (Novacastra. Laboratories, Newcastle, UK), polyclonal anti-Occludin (Santa Cruz Biotechnology) and monoclonal anti-E-cadherin (Invitrogen).

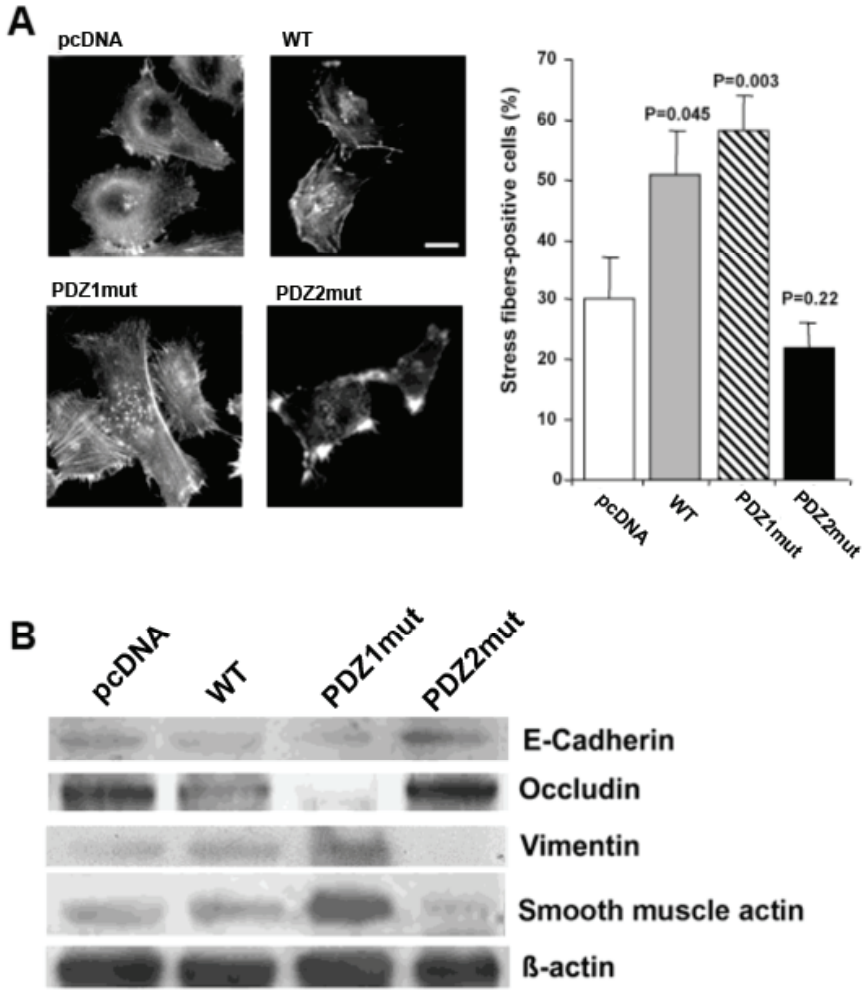

Fig. S5: Calculation of Invadopodial and Podosomal Indices. **(A)** Left panel shows the percent of cells that were positive for at least one invadopodia while the Right panel shows the mean number of invadopodia per cell. Invadopodia Index = percentage of Invadopodia-positive cells (proteolitically-active areas also positive for both actin/cortactin) x mean number of invadopodia/cell. **(B)** Left panel shows the percent of cells that were positive for at least one podosome ring while the right panel shows the mean number of podosome rings per cell. Podosome Index = percentage of podosome-positive cells (ring areas positive for both actin/cortactin) x mean number of podosomes/cell. Very few of these rings were also positive for ECM digestion. Data are presented as mean ± s.e.m.; ANOVA vs pcDNA, * $p<0.01$, ** $p<0.001$, *** $p<0.0001$.

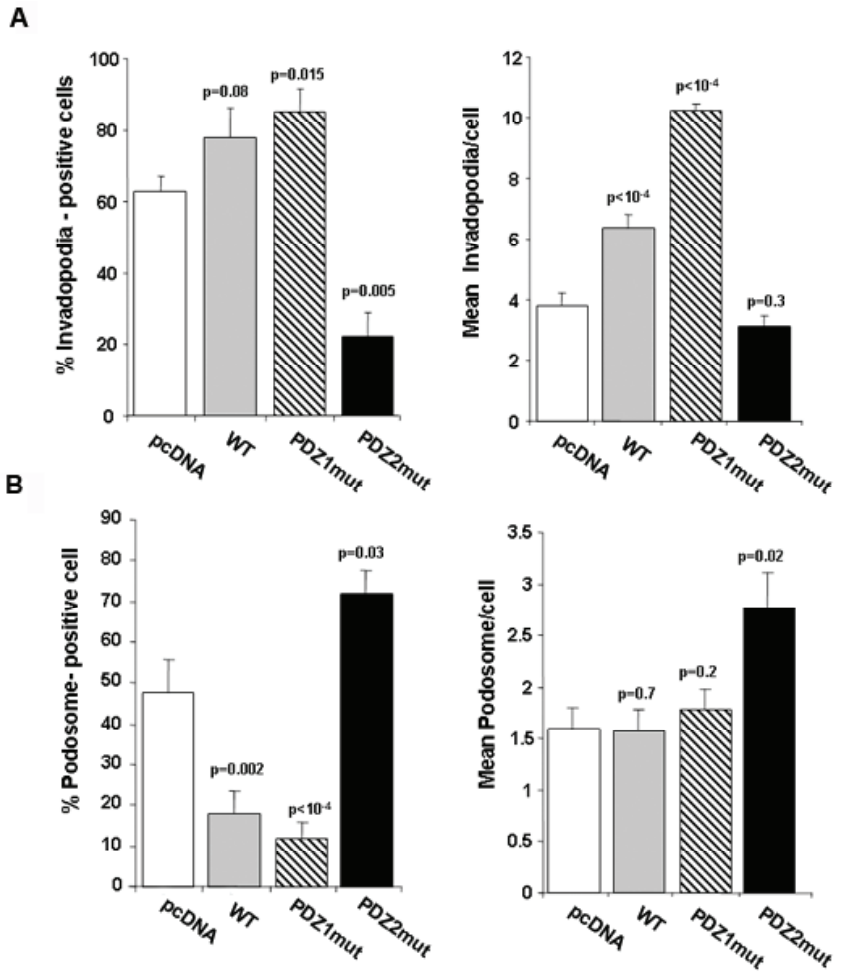

Fig. S6. 3D reconstructions of typical invadopodia (A) and of a podosome ring (B) in a pcDNA and HRF2 cell, respectively. For a better visualization of these structures, the area under the squares were cropped and enlarged in a pcDNA and HRF2 cell, respectively. A series of Z-stack images through both invadopodia and podosomes were acquired and subjected to deconvolution deblurring. Z sections reconstruction of invadopodia revealed that ECM digestion is present and colocalizes throughout these actin/cortactin positive protrusions, while a close visualization of a Z-reconstructed podosome ring shows the F-actin rich core colocalizing with cortactin. Bar, 10μm.

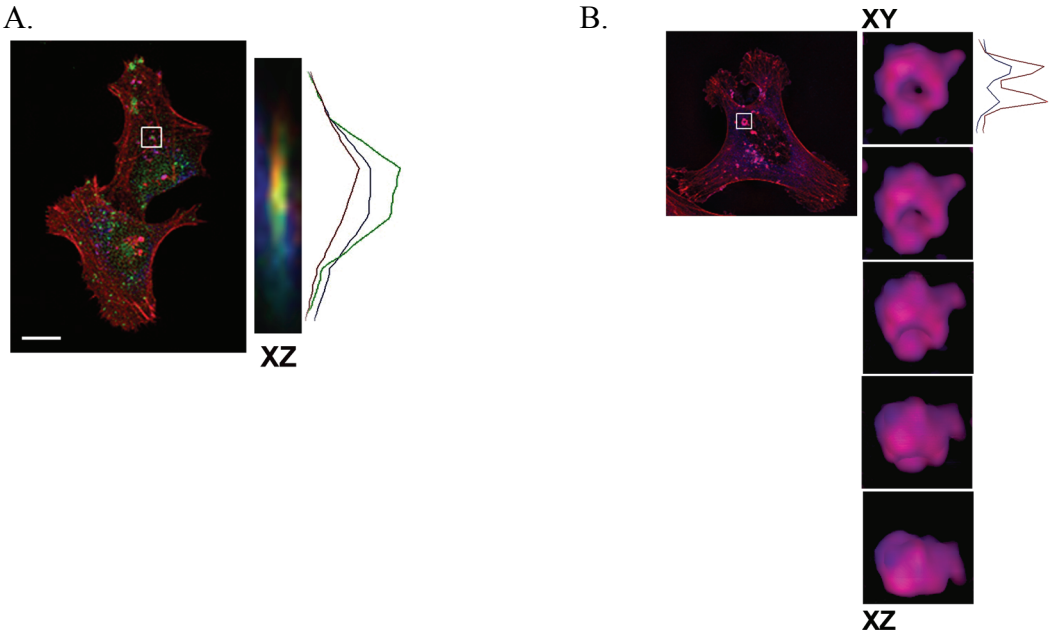

Fig. S7. Analysis of effect of NHERF1 CMs on osteoclastogenesis. Bone marrow from long bones of 7 day-old mice was cultured in 24-well multiplates in the presence of CM from MDA-MB-231 pc-DNA, WT, PDZ1mut and PDZ2mut cells, respectively. After 8 days, cultures were fixed and differentiated osteoclasts were stained for the TRAcP enzyme and counted. The number are the number of TRAcP positive cells per field for 10 fields of three independent experiments. P value vs pcDNA-CM treatments.

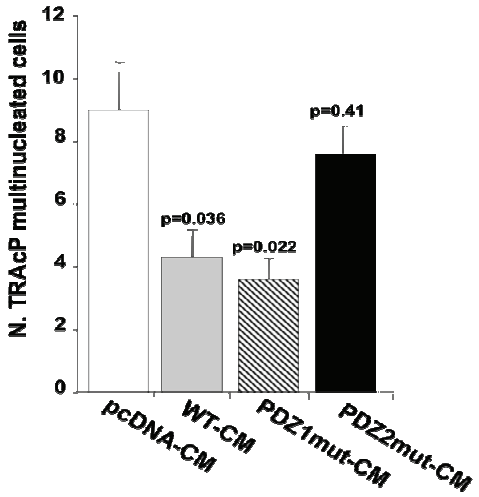

Fig. S8. **Analysis of NHERF1 expression in human normal and breast cancer tissues.** Western blot of NHERF1 protein expression in breast tumor (T) and in its contiguous, non-tumor breast tissue (NT) samples in biopsies from three patients. Proteins extracted from the human breast cancer cell line, MCF-7, represent the positive control positive control. As can be seen in this figure, biopsies from the tumor not only expressed higher levels of NHERF1 but also relatively higher levels of the higher MW band (phospho-NHERF1). This is similar to that previously reported (Cardone et al., 2007).

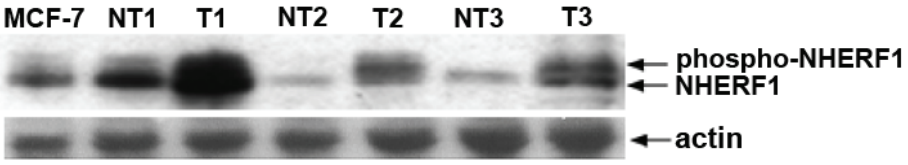

Materials and Methods

Reagents

Porcine skin Gelatin was from Sigma, Matrigel™ Basement Membrane Matrix was from BD Biosciences Discovery Labware (San Jose, CA, USA), Hygromycin B was from Calbiochem. Mouse monoclonal antibody against cortactin (4F11) was from Upstate Cell Signaling Solutions, mouse monoclonal antibody against NHERF1 was from BD Transduction Laboratories, rabbit polyclonal antibody against NHERF1 was from Affinity Bio Reagents, PTEN (A2B1) antibody (sc-7974) was from Santa Cruz, and mouse monoclonal antibody against actin was from Sigma. His-tag, p-AKT, AKT, p-ERK1/2 and ERK½ antibodies were all from Cell Signaling Technology. In immunofluorescence F-actin was identified using Alexa 488-phalloidin from Molecular Probes, Inc. (Eugene, OR). Secondary antibodies were anti-mouse (Sigma) and anti-rabbit (Cell Signaling) HRP-linked antibodies, goat anti-mouse and anti-rabbit Alexa Fluor 568 linked, and donkey anti-mouse Alexa Fluor 647 linked (Molecular Probes).

Immunoblotting and immunofluorescence

Western blot analysis and immunofluorescence assays were performed as described (Cardone et al., 2007). IF-labeled cells were studied using a confocal laser-scanning microscope (C1/TE2000-U; Nikon Instruments) or a Nikon Eclipse TE 2000S epifluorescence microscope. Confocal images were acquired and analyzed as described previously (Busco et al., 2010) using ImageJ software (http://rsb.info.nih.gov/ij/). RGB profiles which demonstrate the intensity fluorescence distribution for each fluorophore were obtained using the ImageJ plugin.

Conditioned Media

For preparation of tumor conditioned medium (CM), cells from each clone were cultured with DMEM containing 10% FBS over-night. Supernatants were removed, and cells were washed with DMEM. Cells were cultured for 30 hours with serum-free DMEM without FBS. After this period the DMEM was centrifuged for 5 minutes at 600Xg to remove cells and large debris. The supernatants were concentrated with Millipore Amicon Ultra-15 (3kDa cut-off) at 3500Xg for 45 minutes at 4°C and protein levels were quantified using the method of Bradford (BioRad) with BSA (Sigma) as the standard**.**

Migration assay

A quantitative measure of the degree of *in vitro* motility of the cells was obtained in BW25 Boyden Chambers (Neuro Probe Inc., Cabin John, MD, USA) using 8 μm polycarbonate membranes (Poretics, Livermore, CA, USA) coated with 5 μg collagen I as previously described (Paradiso et al., 2004). After 4 hours of incubation, cells were fixed and stained (DiffQuick; Baxter, Oakland, CA, USA), those cells that had not transversed the filter were removed and randomly chosen fields were photographed at 100X magnification using a Nikon Eclipse E800 microscope equipped with an MRC-1024 imaging system (Bio-Rad Laboratories, Milano, Italy). The number of cells traversing the filter in four random fields for each filter were counted from these images.

Wound Healing

$2X10^5$ cells from each stable transfected cell line were seeded on a 24-well plate, allowed to grow to a confluent monolayer and then a scratch wound with a yellow plastic pipette tip was made the length of the plate in the center of the monolayer.

After the scratch, the wells were rinsed with DMEM without Hygromycin to remove detached cells. The distance between the wound edges was measured immediately after wounding and 24 hrs later.

Invasion

A quantitative measure of the degree of *in vitro* cellular invasion was measured as the ability to traverse an 8μm polycarbonate membrane coated with 5 μg of Matrigel (Chemicon International, Livermore, CA) as described previously (Cardone *et al*., 2007). The cells were then trypsinized, and 200,000 tumor cells were added in suspension to the upper chamber of the Boyden chamber in which the lower chamber contained 1% serum in culture medium. Culture dishes were returned to the incubator for 8 hr, and then the cells that had traversed the filter were detached and measured according to the manufacturer's instructions. The fluorescent samples were read in a Cary Eclipse fluorescence plate reader (Varian, Palo Alto, CA) at 480/520 nm. Samples without cells but containing all other components were used as blanks. A standard curve of CyQuant dye binding to MDA-MB-231 cells was measured for each cellular clone. The number of cells that had traversed the Matrigel layer was calculated using the standard curve of each treatment.

For 3D evasion assay, 7.5 X 10^3 cells were included in serum-free Matrigel™ drops and incubated for 24 hrs in complete medium (Baldassarre et al., 2005).

Colony formation in soft agar assays

The ability to grow in an anchorage-independent way was measured by the formation of colonies on soft agar. The base layer was prepared with DMEM:0.5% low melting temperature agarose (SeaPlaque, FMC BioProducts, Rockland, Maine). The feed layer was then prepared by resuspending 2X10^4 cells in DMEM:0.25% low melting temperature agarose in the presence of *hygromycin* B and pouring onto the previously prepared base layer (1/2 of the volume of the lower layer). Culture medium was changed every 2 days and colonies counted after 21 days. For each clone, the diameter of the produced colonies was measured and a median value calculated. If the range of diameters for a particular clone was very large, then they were separated into more classes and the median value calculated for each class.

***In Vitro* Angiogenesis and 3D vasculogenic mimicry Network Formation Assays**

Angiogenesis: Adherent human umbilical vein endothelial cells (HUVECs, Lonza) were propagated in Endothelial Basel medium (EBM) with 2% fetal bovine serum, bovine brain extract, hydrocortisone, human endothelial growth factor, and gentamicin/amphotericin B (EGM) in 5% CO_2 in a 37°C incubator. Growth factor supplemented Matrigel™ was allowed to solidify at 37°C for 30 min on a 24-well tissue culture plate and 10^5 HUVEC were then plated in EGM containing concentrated TCM at a ratio of 1 to 5 (v/v) and incubated overnight at 37°C. EBM and EGM served, respectively, as negative or positive controls for the experiments.

Vasculogenic mimicry capillary-like structure formation: Unpolymerized growth factor-reduced Matrigel™ diluted to 7 mg/ml in serum-free medium (DMEM) was mixed with 10^4 cells and plated on dishes containing 22 mm glass. Dishes were carefully inverted for 30 min at 37°C to allow Matrigel™ drops to polymerize, and subsequently complete DMEM plus Hygromycin was added to each dish. After 5 days incubation in a 5% CO_2 humidified atmosphere at 37°C, cell growth and organization were observed through a reverted phase-contrast light microscope (Nikon). Fluorescent staining of cord networks in whole-mount gels and subsequent reconstruction of vessel-like structures in 3D Matrigel™ were performed as follows: medium was removed and the Matrigel™ drops were fixed with 4% PAF for 20 min at room temperature. After washing with PBS, the drops were subsequent incubated at room temperature for 30 min with PBS plus 0.5% Oregon Green® 488 1,2-

dihexadecanoyl-sn-glycero-3-phosphoethanolamine (Oregon Green® 488 DHPE) and washed with PBS.
Angiogenic networks were photographed using in phase contrast while the VM networks were photographed in fluorescence using the same microscope (TE200, Nikon USA, Garden City, NY, USA). Vascular channels were quantified by measuring a set of morphometric parameters such as the number of capillary connections (the mean number of cell branches multiplied for the mean number of nodes where at least three branches meet) and internal lacunae (the empty regions of the field delimited by tubules and cell clusters, i.e., the meshes of the cell network). A branch was counted when at least 3 cells thick and 3 whole cells long. At least five randomly chosen low-power fields were counted per sample.
3-D reconstruction of VM networks was performed by recording specimens under confocal condition by using a Leica TCS SP5 II microscope equipped with a laser-scanning confocal unit containing a He-Ne argon laser (Leica). Samples were viewed through a Planapo 636/1.25 oil immersion objective and images were acquired in the horizontal (x-y) and in the vertical (x-z) planes by the LAS-AF Version 2.2.1 software.

Animals
Four-week-old female immunocompromised BALB/c *nu/nu* mice (Charles River, Milan, Italy) were maintained under sterile conditions and used for all *in vivo* experiments. Procedures involving animals and their care were conducted in conformity with national and international laws and policies (EEC Council Directive 86/609, OJ L 358, 1, Dec. 12, 1987; Italian Legislative Decree 116/92, Gazzetta Ufficiale della Repubblica Italiana n. 40, Feb. 18, 1992; NIH guide for the Care and Use of Laboratory Animals, NIH Publication No. 85-23, 1985), and were approved by our Institutional Review Board.
Animals were monitored daily for body weight, behavior, and survival. Xenografts were monitored daily by measuring the average tumor volume (three axes) using a calliper. After 32 days, mice were sacrificed and tumor mass excised and weighed. Mice were also subjected weekly to radiography (36 KPV for 10 sec) using a Cabinet X-ray system (Faxitron model n.43855A; Faxitron X-Ray Corp., Buffalo Grove, IL) to follow the onset and progression of osteolytic lesions. At the end of the experiment (53 days) mice were sacrificed and subjected to X-ray analysis and to anatomical dissection for evaluation of bone and visceral metastases, respectively. Radiographs were scanned using the Bio-Rad scanning densitometer (Hercules, CA), model GS800, and quantification of the area of interest was done using the Bio-Rad Quantity One® image analysis software.

Xenograft Histology
Subcutaneous tumors were fixed in 4% formaldehyde in 0.1 M phosphate buffer, pH 7.2, and embedded in paraffin. Sections were cut using a Reichert-Jung 1150/Autocut microtome. Slide-mounted tissue sections (4 μm thick) were deparaffinized in xylene and hydrated serially in 100%, 95%, and 80% ethanol. Endogenous peroxidases were quenched in 3% H_2O_2 in PBS for 1 hour, then slides were incubated with the anti-Ki67 primary antibody for 1 hour at room temperature. Sections were washed three times in PBS, and antibody binding was revealed using the Ultra-Vision Detection System anti-Polyvalent HRP/DAB kit according to the manufacturer's instructions (Lab Vision; Scaffold, UK).

References of Supplemental Material

Baldassarre, G., Belletti, B., Nicoloso, M.S., Schiappacassi, M., Vecchione, A., Spessotto, P., Morrione, A., Canzonieri, V., and Colombatti, A. (2005). p27(Kip1)-

stathmin interaction influences sarcoma cell migration and invasion. Cancer Cell *7*, 51-63.

Busco, G., Cardone, R.A., Greco, M.R., Bellizzi, A., Colella, M., Antelmi, E., Mancini, M.T., Dell'Aquila, M.E., Casavola, V., Paradiso, A., and Reshkin, S.J. (2010). NHE1 promotes invadopodial ECM proteolysis through acidification of the peri-invadopodial space. FASEB J *24*, 3903-3915.

Cardone, R.A., Bellizzi, A., Busco, G., Weinman, E.J., Dell'Aquila, M.E., Casavola, V., Azzariti, A., Mangia, A., Paradiso, A., and Reshkin, S.J. (2007). The NHERF1 PDZ2 domain regulates PKA-RhoA-p38-mediated NHE1 activation and invasion in breast tumor cells. Mol Biol Cell 18, 1768-1780.

Chao, Y.L., Shepard, C.R., and Wells, A. Breast carcinoma cells re-express E-cadherin during mesenchymal to epithelial reverting transition. Mol Cancer 9, 179.

Hugo, H., Ackland, M.L., Blick, T., Lawrence, M.G., Clements, J.A., Williams, E.D., and Thompson, E.W. (2007). Epithelial--mesenchymal and mesenchymal--epithelial transitions in carcinoma progression. J Cell Physiol 213, 374-383.

Karthikeyan, S., Leung, T., Ladias, J.A. (2002) Structural determinants of the Na+/H+ exchanger regulatory factor interaction with the beta 2 adrenergic and platelet-derived growth factor receptors. J Biol Chem. 277(21):18973-18978.

Karthikeyan, S., Leung, T., Birrane, G., Webster, G., Ladias, J.A. (2001) Crystal structure of the PDZ1 domain of human Na(+)/H(+) exchanger regulatory factor provides insights into the mechanism of carboxyl-terminal leucine recognition by class I PDZ domains. J Mol Biol. 308(5):963-973

Khundmiri, S.J, Weinman, E.J., Steplock, D., Cole, J., Ahmad, A., Baumann, P.D., Barati, M., Rane, M.J., Lederer, E. (2005) Parathyroid hormone regulation of NA+,K+-ATPase requires the PDZ 1 domain of sodium hydrogen exchanger regulatory factor-1 in opossum kidney cells. J Am Soc Nephrol. 16(9):2598-2607.

Khundmiri, S.J, Ahmad, A., Bennett, R.E, Weinman, E.J, Steplock, D., Cole, J., Baumann, P.D., Lewis, J., Singh, S., Clark, B.J. Lederer, E.D. (2008) Novel regulatory function for NHERF-1 in Npt2a transcription. Am J Physiol Renal Physiol. 294(4):F840-849.

Paradiso, A., Cardone, R.A, Bellizzi, A., Bagorda, A., Guerra, L. Tommasino, M., Casavola, V., Reshkin, S.J. (2004). The Na+-H+ exchanger-1 induces cytoskeletal changes involving reciprocal RhoA and Rac1 signaling, resulting in motility and invasion in MDA-MB-435 cells. Breast Cancer Res 6, R616-628.